W. -T. Hsu and C. T. -C. Nguyen, "Stiffness-compensated temperature-insensitive micromechanical resonators," *Tech. Digest*, 2002 IEEE Int. Micro Electro Mechanical Systems Conf., Las Vegas, Nevada, Jan. 20-24, 2002, pp. 731-734.

STIFFNESS-COMPENSATED TEMPERATURE-INSENSITIVE MICROMECHANICAL RESONATORS

Wan-Thai Hsu[1] and Clark T.-C. Nguyen
Center for Wireless Integrated Microsystems
Department of Electrical Engineering and Computer Science
University of Michigan, Ann Arbor, MI 48109-2122, U.S.A.

ABSTRACT

Polysilicon μmechanical resonators utilizing a novel temperature-dependent electrical stiffness design technique to compensate for temperature-induced frequency shifts have been demonstrated with greatly reduced temperature coefficients (TC_f's) on the order of –0.24 ppm/^{o}C, which is 67 times smaller than exhibited by previous uncompensated resonators. With this new resonator design, the total frequency excursion over a 300K to 380K range has been reduced from 1,280 ppm for an uncompensated device [1] to only 18 ppm, which for the first time, is now small enough to erase lingering concerns regarding the temperature stability of MEMS-based resonators for use in communication applications.

I. INTRODUCTION

Demonstrations over recent years of polysilicon vibrating micromechanical ("μmechanical") resonators with frequencies in the hundreds of MHz that retain Q's around 10,000 [2] have generated great interest in the use of these devices as building blocks for the low-loss bandpass filters and ultra-stable reference oscillators needed in communication transceivers. If feasible, the use of such devices could lead to both substantial size reduction and power savings in communication transceivers [3], especially when alternative architectures are used that take advantage of the tiny size and zero dc power consumption of μmechanical resonators [4].

Of the various transceiver functions addressable via MEMS technology [4], the reference oscillator is among the most difficult to realize, since its stability specifications are quite demanding. To date, although the demonstrated Q's of μmechanical resonator devices are theoretically sufficient to satisfy the short-term stability needs of reference oscillators [5], their aging stability remains little tested, and their temperature stability, although sufficient for filter applications, falls well short of the marks required by oscillators. In particular, as illustrated in Fig. 1, the temperature excursion for an uncompensated clamped-clamped beam ("CC-beam") polysilicon μmechanical resonator over a 27 to 127^{o}C range is more than 15X larger than that of the worst AT-cut crystal.

Pursuant to improving the thermal stability of μmechanical resonators, this paper presents an electrical stiffness-based temperature compensation technique, in which a dc-biased electrode-to-resonator gap spacing is strategically designed to change with temperature, thereby introducing a temperature-dependent electrical stiffness that produces a frequency shift to counteract frequency shifts caused by inherent material and mechanical temperature dependences. Using this design technique, polysilicon μmechanical resonators are demonstrated with greatly reduced temperature coefficients (TC_f's) on the order of –0.24 ppm/^{o}C, which is 67 times smaller than exhibited by previous uncompensated resonators. With this new resonator design, the total frequency excursion over a 300K to 380K temperature range has been reduced from 1,280 ppm for an uncompensated device [1] to only 18 ppm. In addition to outright better performance, this technique offers numerous other advantages over previous compensation methods, including: (1) no dc power consumption; (2) voltage-control of the temperature coefficient; (3) ease of fabrication, which makes it flexible enough to use on a variety of different resonator designs; and (4) less susceptibility to stress relaxation (which is a potential problem for a previously reported geometric-stress compensation method [7]).

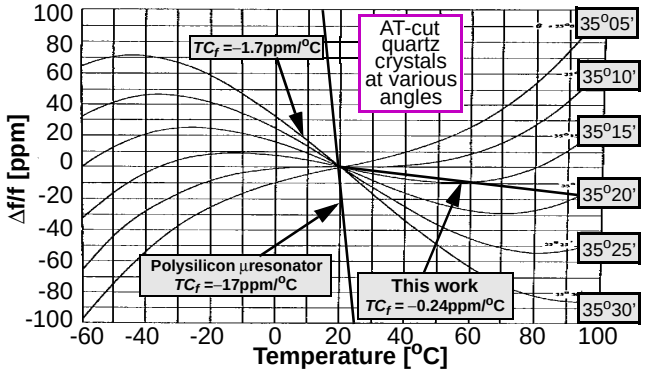

Fig. 1: Plots of fractional frequency change versus temperature comparing AT-cut quartz crystals at various angles [6] with polysilicon μmechanical resonators.

II. ELECTRICAL STIFFNESS COMPENSATION

Figure 2(a) presents a cross-sectional schematic conveying the basic concept behind the stiffness-compensated temperature-insensitive μresonator, indicating key components and specifying a preferred bias and excitation configuration. As shown, this device consists of a polysilicon CC-beam resonator, over which a metal electrode spaced a distance d_{o2} (e.g., 1000Å) above the beam has been added as the key instrument for temperature compensation. To simplify this initial discussion, the anchoring structure for this top electrode is drawn such that it can freely expand in the lateral direction without introducing compressive stresses that might bend the electrode.

With this simplification, the overhead electrode in Fig. 2 is then effectively supported by blocks free to expand in the vertical direction. For stiffness compensation, the material comprising these support blocks is chosen to have a thermal expansion coefficient larger than that of the structural material of the mechanical resonator and its anchors. With this selection of materials, when the temperature is increased, expansions are such that the bottom side of the top electrode moves vertically upwards faster than the top of the resonator beam, resulting in a net increase in the top electrode-to-resonator gap spacing d_{o2}, as shown in the higher temperature cross-section of Fig. 2(b). This

[1] Now with Discera, Inc., 755 Phoenix Drive, Ann Arbor, MI 48108, U.S.A. email: wanthaihsu@discera.com

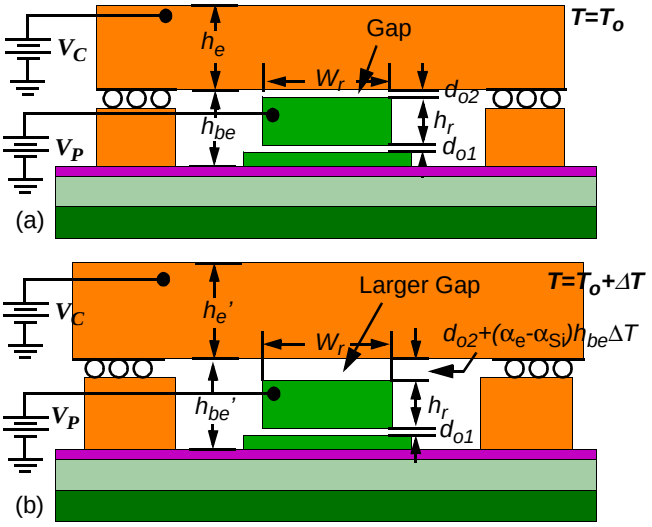

Fig. 2: Cross-sectional schematics of a stiffness-compensated μmechanical resonator (a) at temperature T_o; and (b) at an elevated temperature $T_o+\Delta T$.

increase in the gap spacing then leads to a decrease in the top-electrode-to-resonator electrical spring constant and a corresponding increase in the resonance frequency, which then counteracts the decrease in frequency caused mainly by Young's modulus temperature dependence. Accounting for this mechanism, the expression for the temperature coefficient of the resonance frequency can be written as

$$TC_f = \frac{(\alpha_{E_r} + \alpha_r)}{2} + \frac{3}{2}\frac{(V_P - V_C)^2 \varepsilon_o A_{o2}}{d_{o2}^4 k_{r1}}(\alpha_e - \alpha_r)h_{be} \quad (1)$$

where α_{Er} is the temperature coefficient of the Young's modulus of the resonator material (note that it is negative); V_C is a control voltage applied to the top electrode; k_{r1} is the spring constant of the resonator beam including the effects of the electrical stiffness k_{e1} due to the bottom electrode ($k_{r1}=k_m-k_{e1}$, where k_m is the unbiased mechanical stiffness); h_{be} is the gap between the substrate and the bottom of the top electrode; ε_o is the permittivity in vacuum; and α_e and α_r are the thermal expansion coefficients of electrode and resonator, respectively.

Since the electrical stiffness generated across an electrode-to-resonator gap depends strongly on not only the gap spacing d_{o2}, but also on the voltage applied across the gap (V_P–V_C), the TC_f given by (1) also exhibits a strong dependence on (V_P–V_C). In fact, by appropriate adjustment of V_C, the electrical stiffness as a function of temperature can be conveniently optimized to more effectively null the TC_f of the resonator beam—a distinct advantage over other compensation methods.

III. PRACTICAL STIFFNESS-COMPENSATED RESONATOR DESIGNS

In practical renditions, the stiffness-compensating design of Fig. 2 suffers to some degree from top electrode bending caused mainly by compressive stresses exerted by the anchors supporting the top electrode. If the top electrode is allowed to bend, the frequency versus temperature function will deviate from the linear behavior predicted by (1). In particular, depending upon the degree and rate of bending, the frequency versus temperature curve might look parabolic, or might start curving at some high threshold temperatures.

Figures 3(a) and (b) present perspective-view schematics

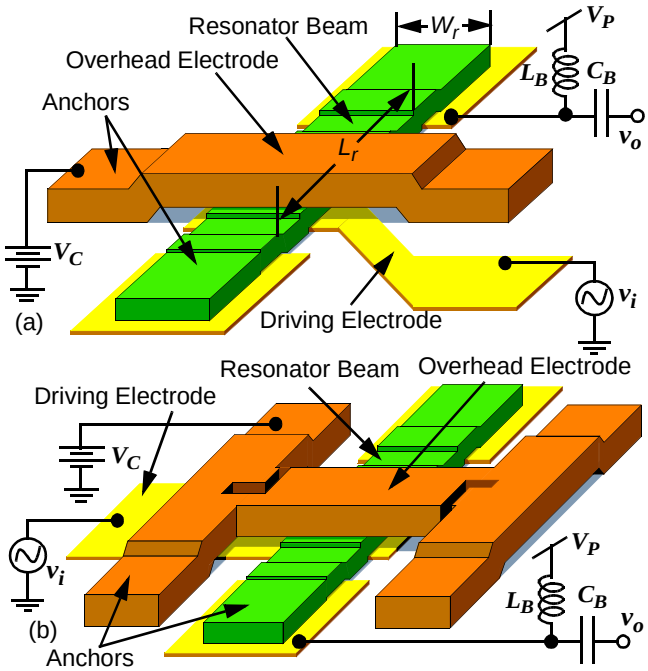

Fig. 3: Perspective-view schematics of stiffness-compensated vertical μmechanical resonators using (a) a simple fixed-fixed beam top electrode; and (b) a stress-relieving top electrode.

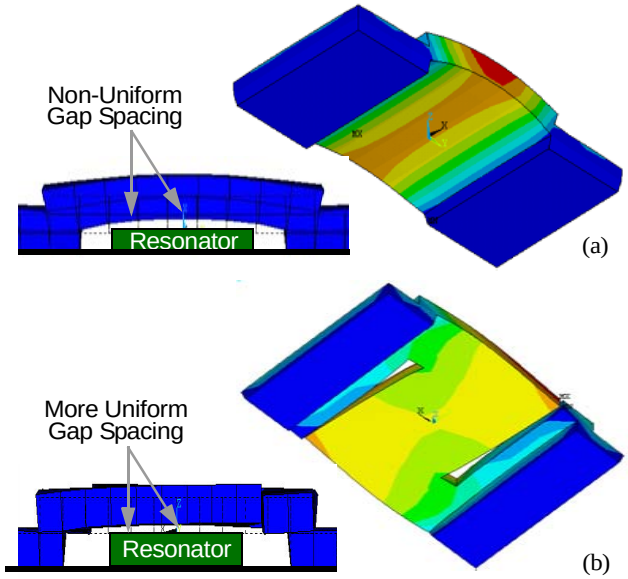

Fig. 4: FEA predicting thermal expansion-induced bending of the top electrode under elevated temperature for (a) the design Fig. 3(a); and (b) the stress-relieving design of Fig. 3(b).

of the two practical renditions of stiffness-compensated resonators evaluated via this work. The design of Fig. 3(a) constitutes the most straightforward design, in which conventional fixed-fixed anchors are used and no effort is made to mitigate bending of the top electrode. The design of Fig. 3(b) introduces both split electrodes and slits in the top electrode beam in an attempt to eliminate both vertical- and axial-stress-induced beam bending. As described in [7], the use of split electrodes reduces thermally-induced expansion differences along the thickness of anchors, thus, decreasing vertical-stress-induced beam bending. Meanwhile, the slits mitigate axial-stress-induced bending.

Figure 4 presents FEA simulations using ANSYS predict-

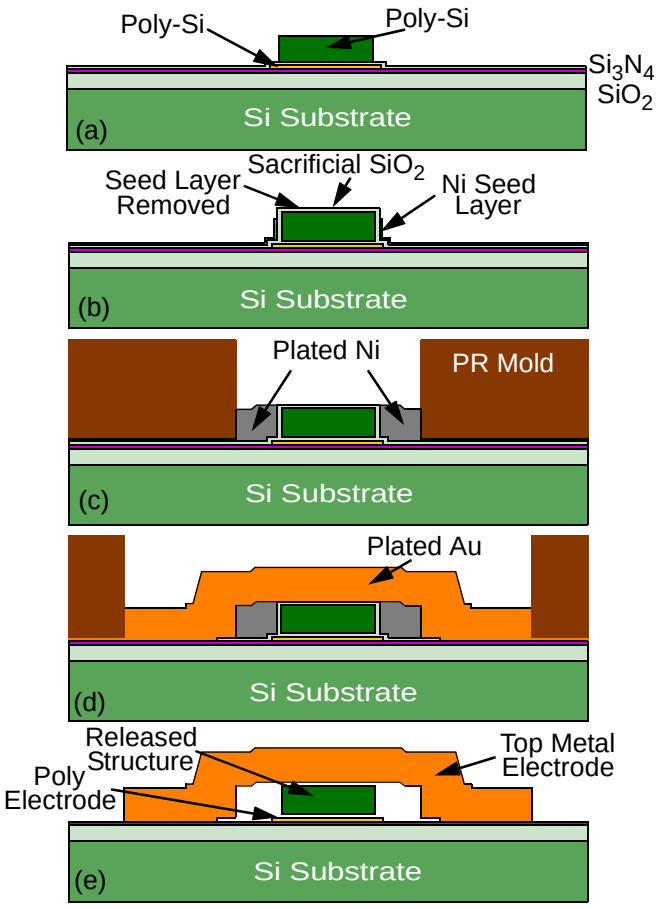

Fig. 5: Process flow for the stiffness-compensated μmechanical resonators of this work.

ing the degree of bending expected at an elevated temperature of 100°C for each of the design variants in Fig. 3. As expected, the stress-relieved design of Fig. 3(b) performs better, with less than 10Å of edge-to-center bending of the top electrode, as compared with the unrelieved design of Fig. 3(a), which exhibits more than 60Å of edge-to-center bending.

IV. FABRICATION PROCESS

The fabrication process used to attain stiffness-compensated μmechanical resonators differs from that of a conventional, small-gapped surface μmachining process [1] only in steps associated with top electrode construction, all of which can be considered as part of a post-resonator process module. Thus, unlike a previous mechanical compensation technique that complicated the design of the resonator [7], the present method allows the resonator and temperature compensation to be designed and implemented almost independently.

Figure 5 presents the cross-sectional fabrication process flow for the stiffness-compensated structures of Fig. 3. As shown, the process begins with a standard high frequency vertical resonator surface micromachining process [1] that yields the cross-section of Fig. 5(a), where sacrificial oxide and oxide etch mask layers still remain around a patterned resonator structure. At this point, the process deviates from that of conventional surface-micromachining, in that instead of an HF release step, a 700Å/300Å Ti/Ni electroplating seed layer is evaporated and removed from the tops of resonators via a thick PR/etch back process (described in [8]) to yield the cross-section of Fig. 5(b). A plating mold is then formed between the edges of a thick patterned PR and the resonator structure itself, and a Ni sacrificial spacer layer is electroplated through it in a 50°C sulfamate solution to yield the cross-section of Fig. 5(c). After removal of the mold and seed layer used to form the sacrificial layer, another seed layer of Cr/Au/Cr (200Å/400Å/200Å) and PR mold are applied, and Au is then electroplated to form the top electrode structure as shown in Fig. 5(d). The mold and the seed layer for this step are next removed using PRS-2000 and CR-14/GE8148/CR-14 solutions, and the Ni spacer is removed using a $CH_3COOH:HNO_3:H_2SO_4$=5:5:2 solution. Finally, both the μmechanical resonator and top electrode are released simultaneously in a solution of 49 wt. % concentrated HF, leaving the free-standing final cross-section of Fig. 5(e).

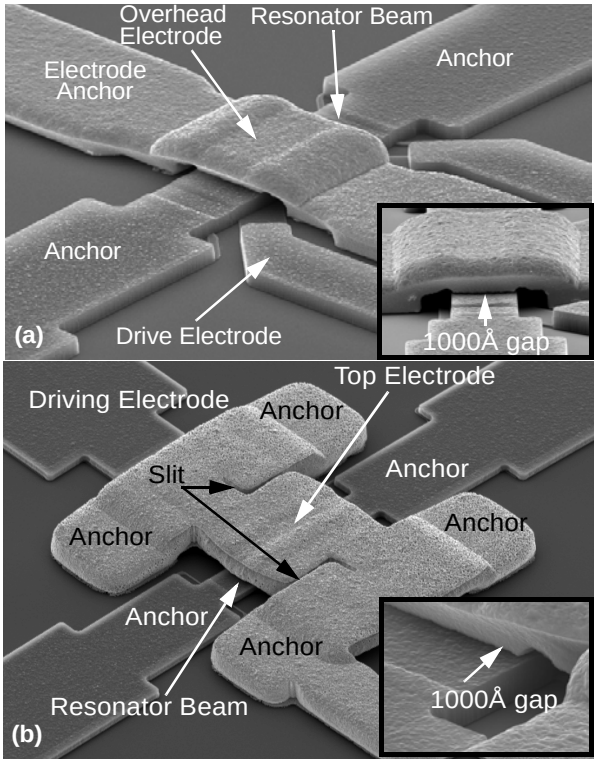

Fig. 6: SEMs of fabricated stiffness-compensated temperature-insensitive μmechanical resonators with (a) a simple fixed-fixed top electrode, and (b) a stress-relieving top electrode.

V. EXPERIMENTAL RESULTS

Electrical stiffness-compensated CC-beam resonators were designed and fabricated via the process detailed above. Figures 6(a) and (b) present scanning electron micrographs (SEMs) of fabricated resonators sporting the designs of Fig. 3. The slits in the top electrode of Fig. 6(b) are clearly visible. Although their top electrode designs differed, the performance-determining dimensions (e.g., L_r, d_{o2}, etc.) for each variant were identical, and these are summarized in the inset of Fig. 7 (to be discussed) with reference to Figs. 2 and 3.

A custom-built vacuum chamber evacuated by a turbo molecular pump was used to supply the low pressure (down to 50 μTorr) environment needed to attain resonator Q's in the thousands [1]. Dies containing micromechanical devices were first mounted onto pc boards containing biasing components, then inserted into the vacuum chamber for testing, where special feedthroughs allowed electrical connection to outside measurement instrumentation. The pc boards and vacuum chamber feedthrough interface used for this work differed from those

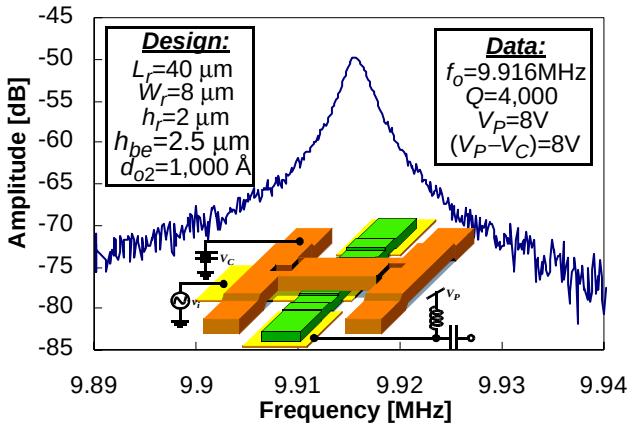

Fig. 7: Measured frequency spectrum for the ~10 MHz stiffness-compensated µmechanical resonator of Fig. 6.

Table I: µResonator Performance Between 300K~380K

Performance	Uncomp. CC-Beam [1]	Geom. Stress Ref [7]	This work: Electrode w/o stress relief	This work: Electrode w/ stress relief
TC_f [ppm/^{o}C]	–16	–2.5	0.6(300~360K)	–0.24
Total Δf [ppm]	1,280	196	101(300~380K)	17.8

previously used for frequency characterization of micromechanical resonators in that special provisions were made to allow insertion of an MMR Technologies temperature-controllable cantilever into the vacuum chamber, and to realize a low thermal-resistance connection from the board-loaded resonator die to the MMR cantilever.

Figure 7 presents the frequency characteristic for a ~10 MHz version of the device of Fig. 3(b), measured using the above set-up and an HP8753 Network Analyzer. Here, a Q of 4,000 is achieved for a center frequency peak of 9.916 MHz, which is on par with previous CC-beams in this frequency range. Each of the design variants in Fig. 3 exhibited similar Q's, verifying that in general micromechanical resonator performance is not greatly impacted by the introduction of electrical stiffness-compensation.

Figures 8(a) and (b) present plots of fractional frequency change versus temperature for each of the resonators of Fig. 6 with varying values of applied dc-bias (V_P–V_C) across the top electrode-to-resonator gap. Clearly, the slope of the frequency versus temperature curve is adjustable via V_C in each case. In addition, the linearity of each curve is seen to be a function of the amount of stress relief provided by the particular top electrode design, with the best linearity (and thus, best overall performance) seen for the design of Fig. 3(b), which featured the most stress relief. For this resonator, the frequency versus temperature curve is flattest when (V_P–V_C)=8V, for which a TC_f of –0.24 ppm/^{o}C is exhibited and a total frequency excursion of only 17.8 ppm from 300K to 380K is achieved—the best to date for any micromechanical resonator without assistance from active electronics. Table I compares performance data for the electrical stiffness-compensated designs in this work with that for previous resonators with and without compensation.

The data for the (V_P–V_C)=8V curve of Fig. 8(b) is also plotted in Fig. 1, showing just how well the temperature-dependence of the stiffness-compensated resonator of Fig. 6(b) compares with that of the best AT-cut quartz crystals. As can be seen, the temperature independence of the stiffness-compen-

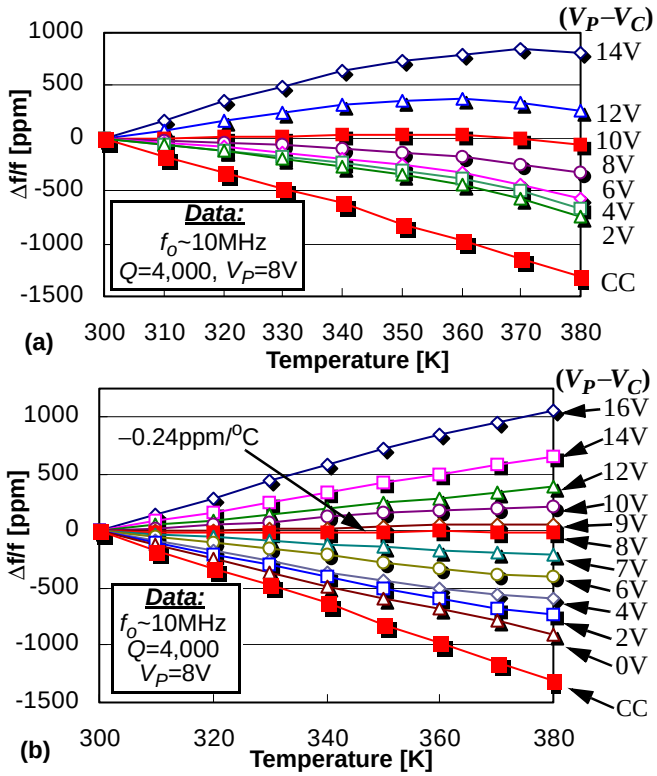

Fig. 8: Measured plots of fractional frequency change versus temperature for stiffness-compensated µmechanical resonators under various control voltages V_C for the designs of (a) Fig. 6(a), with the simple electrode; and Fig. 6(b), with the stress relieving electrode.

sated resonator is arguably just as good as that of the best AT-cut quartz crystal, and is perhaps actually even better, since its curve is much more linear, hence easier to further compensate out using active compensation circuitry.

VI. CONCLUSIONS

Via the described stiffness-compensation design technique, the temperature stabilities of µmechanical resonators have been reduced to levels rivaling that of the best AT-cut quartz crystals, and this constitutes a major step towards the use of these devices in stringent communications reference oscillator applications. Although the demonstrated performance is extremely encouraging, it should be mentioned that work towards establishing µmechanical resonators as practical frequency references is still unfinished, since hysteresis in the temperature curves is yet untested, and sufficient aging and thermal stability must still be demonstrated under packaged environments. Work towards these ends is ongoing.

Acknowledgments: This work was supported by DARPA under Grant No. F30602-97-2-0101.

References:

[1] K. Wang, *et al.*, *JMEMS*, vol. 9, no. 3, pp. 347-360, Dec. 1999.
[2] J. R. Clark, *et al.*, IEDM'00, pp. 493-496.
[3] C. T.-C. Nguyen, Int. MEMS Wkshp'01, Singapore, July 4-6, 2001, pp. 21-34.
[4] C. T. -C. Nguyen, Topical Mtg. on Silicon Monolithic Integrated Circuits in RF Systems, Sept. 12-14, 2001, pp. 23-32.
[5] S. Lee, *et al.*, Transducers'01, pp. 1094-1097.
[6] M. E. Frerking, *Crystal Oscillator Design and Temperature Compensation*. Van Nostrand, 1978.
[7] W.-T. Hsu, *et al.*, IEDM'00, pp. 399-402.
[8] W.-T. Hsu, *et al.*, MEMS'01, pp. 349-352.